Journal of Thermal Analysis and Calorimetry (2021) 143:1273–1289
https://doi.org/10.1007/s10973-020-09850-1

On the hydrothermal features of radiative Fe_3O_4–graphene hybrid nanofluid flow over a slippery bended surface with heat source/sink

Nilankush Acharya[1] · Fazle Mabood[2]

Received: 14 March 2020 / Accepted: 15 May 2020 / Published online: 26 May 2020

Abstract

The present investigation concentrates on the hydrothermal features of both hybrid nanofluid and usual nanofluid flow over a slippery permeable bent structure. The surface has also been considered to be coiled inside the circular section of radius R. Ferrous and graphene nanoparticles along with the host fluid water are taken to simulate the flow. The existence of heat sink/source and thermal radiation are incorporated within the system. Resulting equations are translated into its non-dimensional form using similarity renovation and solved by the RK-4 method. The consequence of pertinent factors on the flow profile is explored through graphs and tables. Streamlines and isotherms for both hybrid nanofluid and usual nanofluid are depicted to show the hydrothermal variations. The result communicates that temperature is reduced for curvature factor, whereas velocity is found to be accelerated. Heat transfer is intensified for thermal Biot number, and the rate of increment is higher for hybrid nanosuspension. Velocity and temperature are intensified for enhanced nanoparticle concentration. The heat transport process is decreased for the heat source parameter, but the reduction rate is comparatively slower for hybrid nanofluid.

Keywords Hybrid nanofluid · Bended surface · Surface slip · Suction/injection · Nonlinear radiation · Heat source/sink

Mathematics Subject Classification 76W05

List of symbols

(u, v)	Velocity components (m s^{-1})
r, s	Spatial coordinates (m)
a	Stretching constant (s^{-1})
U_w	Stretching velocity (m s^{-1})
a	Stretching rate (s^{-1})
R	Radius of curvature (m)
T_w	Temperature of the surface (K)
T_∞	Temperature away from surface (K)
T	Hybrid nanofluid temperature (K)
ρ	Density (kg m^{-3})
μ	Dynamic viscosity (kg m^{-1} s^{-1})
κ	Thermal conductivity (W m^{-1} K^{-1})
ρC_p	Heat capacitance (J m^{-3} K^{-1})
σ	Electrical conductivity (Ω^{-1} m^{-1})
B_0	Magnetic field ($\Omega^{1/2}$ m^{-1} $s^{-1/2}$ $kg^{1/2}$)
q_r	Radiative heat flux (kg s^{-3})
σ^*	Stefan Boltzmann constant (W m^{-2} K^{-4})
k^*	Mean absorption coefficient (m^{-1})
L	Velocity slip factor (m)
v_w	Suction/injection velocity (m s^{-1})
h	Convective heat transport coefficient (W m^{-2} K^{-1})
ϕ	Nanoparticle volume fraction
Q	Heat source or sink
$K = \sqrt{\frac{a}{\nu_f}}R$	Curvature parameter
$L_{slip} = L\sqrt{\frac{a}{\nu_f}}$	Velocity slip parameter
$\Pr = \frac{\mu_f (\rho C_p)_f}{\rho_f \kappa_f}$	Prandtl number
$M = \frac{\sigma_f B_0^2}{a \rho_f}$	Magnetic parameter
$S = -\frac{v_w}{\sqrt{a \nu_f}}$	Suction/injection parameter
$\mathrm{Bi} = \frac{h_f}{\kappa_f}\sqrt{\frac{\nu_f}{a}}$	Biot number
$N = \frac{4\sigma^* T_\infty^3}{3k^* \kappa_f}$	Radiation parameter
$\theta_w = \frac{T_w}{T_\infty}$	Temperature ratio parameter

✉ Nilankush Acharya
nilankushacharya@gmail.com

Fazle Mabood
mabood1971@yahoo.com

1 Department of Mathematics, Jadavpur University, Kolkata, West Bengal 700032, India

2 Department of Information Technology, Fanshawe College, London, ON, Canada

$\lambda = \frac{Q}{a(\rho c_p)_f}$	Heat source/sink parameter
Nu	Nusselt number
C_f	Skin friction
Nu_r	Reduced Nusselt number
C_{fr}	Reduced skin friction
$Re_s = \frac{as^2}{\nu_f}$	Local Reynold's number

Subscripts

f	Base fluid
nf	Nanofluid
hnf	Hybrid nanofluid
1, 2	First and second nanoparticle, respectively

Introduction

Thermal management and analysis of heat transport acquired a major concern for engineers, scientists and researchers due to its multipurpose uses in the technological fields or industries that deals with high thermal energy. Thus, due to the rising technologies and energy production, engineers are claiming to have an efficient lubricants and coolants. Our conventional fluids like water, kerosene and glycerol are not so effective to satisfy those needs because of their low thermal conductivity. Their heat transport capabilities are limited. But, the addition of tiny metallic particles (whose diameter ranges from 1 to 100 nm) within the base medium would significantly enhance the thermal conductivity of the resulting liquid and thus becomes a most promising candidate to transfer heat. Such fluids are marked as "nanofluid". It was coined by Choi [1]. From then, extensive investigations [2–4] are going on to explore the hidden application of nanofluids. Sheikholeslami [5] addressed the entropy and exergy analysis of nanofluidic transport through porous medium in the presence of Lorentz force. He included non-Darcy model to simulate the flow. Results indicated that Bejan number detracts with the reduction in the permeability. Sheikholeslami et al. [6] experimentally studied the application of nanorefrigerant for boiling heat transport. Nanorefrigerant (R600a/Oil/Cuo) is included in the study. They reported that heat transport is increased for enhanced mass flux. Sadeghi et al. [7] communicated the impact of surface reactions in electrokinetically actuated microfluidic devices. Leading equations were solved using finite difference scheme. They found a concentration wave for sufficiently long microchannels. Effects of shear rate-dependent rheology on surface reactions and mass transfer in microfluidic devices was illustrated by Sadeghi et al. [8]. Outcomes suggested that maximum rheology effect was confirmed for square section channels. The hydrothermal and heat transfer characteristics are investigated by several researchers for the flow over diverse geometries [9–20].

Recently, an extended version of nanofluid, i.e. "hybrid nanofluid", has snatched attention from so many researchers worldwide. Hybrid nanofluid is the dispersion of double metallic nanoparticles within the host fluid. Because of double metallic additives, hybrid nanofluid appears to be the most efficient candidate for heat transfer and coolant issues [21, 22]. It has useful applications in different sectors like the solar receiver, nuclear reactor, microbial fuel cell, thermal storage, glass production, aerospace technologies, biomedical applications, heat exchangers, defence purpose, industrial cooling medium, etc. [23–25]. Studies of the hydrothermal behaviour of hybrid nanofluid or usual nanofluid over stretched textures are extremely noteworthy due to its wide range of truthful applications in diverse fields of engineering and industrial sectors like glass blowing, drawing of wires, hot rolling, paper production, fibre spinning, etc. One can easily trace out such different aspects of nanofluid flow over stretched surface through the open literature [26–30]. Natural convective magnetized hybrid nanofluid flow over a stretched surface considering the viscosity variations was addressed by Manjunatha et al. [31]. They reported that increasing volume fraction aids temperature and velocity to increase and hybrid nanofluid becomes the most promising heat transfer medium as compared to usual one. Hayat and Nadeem [32] illustrated the heat transport amplification of copper oxide and silver water-based hybrid nanofluid stream crossing over a linearly stretched surface. Yousefi et al. [33] disclosed the stagnation flow of titanium–copper water hybrid nanosuspension over a wavy cylinder. They claimed that thermal features of hybrid nanofluid are superior to that of ordinary nanofluid. Entropy analysis of thermally dissipative copper–alumina water hybrid nanofluid over a thin needle was carried out by Afridi et al. [34]. They found that hybrid nanofluid's velocity is less as compared to usual one. Nadeem et al. [35] revealed the revolving hybrid MWCNT–SWCNT nanofluid flow over a convectively heated stretched surface in the presence of heat absorption/generation. Result extracts that hybrid nanofluid provides improved heat transport. The related literature can be found in [36–42].

Literature survey ensures that the investigation of fluid flow over the curved surface has been hardly analysed. Examples of two-dimensional fluid running over bent surface are the liquid interface, similar to the interfaces between foam bubbles, molecular films or aerosol droplets. Also, one real-life scenario of liquid flow over the curved face is the soap films that are broadly used to scrutinize classical 2D hydrodynamic phenomena. Another real technological application of coiled surface is explored through the curved jaws of stretchable assembling equipments in industries. One microbiological instance is revealed through the liquid motion over lipid bilayer membranes over large number of cells. Lipid bilayers do reveal hydrodynamic characteristics like diffusion and viscosity, and such outcomes are ensured by miscellaneous experiments. Viscous liquid flow over stretched curved sheet was studied by Sajid et al. [43]. Viscous flow over nonlinear stretched sheet was examined by Sanni et al. [44]. Shaiq and Maraj [45] marked the induced magnetization effect of CNT–propylene glycol-based nanoliquid flow over a bent surface. Result concluded that skin friction enhances for nanoparticle concentration, but reduces for curvature. Imtiaz et al. [46] discussed the convectively heated ferrofluid flow over curved sheet. They included heterogeneous homogeneous reaction to address the hydrothermal variations inside the boundary regime. Entropy analysis for copper–alumina water hybrid nanoliquid stream over curved texture was carried out by Afridi et al. [47]. They established that less entropy generation is ensured for usual nanofluid as compared to hybrid one. Saba et al. [48] disclosed the thermal characteristics of CNT water-based nanofluid flow over curved sheet. The internal heat generation concept was conceived by them. The study explores that heat flux rate is enhanced for curvature factor, but declines for heat source. More studies are in [49–58].

Being inspired from the above researches, in this communication we have depicted the hydrothermal variations of magnetite–graphene water-based hybrid nanoliquid flow over a slippery bended surface. Radiation and the existence of heat source/sink are included to explore the hydrothermal integrity of the flow. Resulting equations have been solved using classical RK-4 procedure, and the outcomes convey the variations for both hybrid and usual nanoliquids. The graphene nanoparticles have useful applications in solar cells, microbial fuel cells, tissue engineering, biomedical applications, drug delivery, cancer therapy, biosensing, etc. Owing to their ultrahigh surface area, graphene nanoparticles are the best candidate for drug or gene delivery applications. Additionally, magnetic nanoingredients have drawn noteworthy consideration for their biomedical functions; among them, iron oxide nanoparticles prove to be mostly satisfactory due to their fundamental compositions that turns them biocompatible and degradable. Thus, the composition of Fe_3O_4–graphene hybrid nanofluid will enhance the functions of drug delivery, cancer therapy for improved applicability in biotechnology. To the best of our knowledge, no investigation has been forwarded that sheds light on the mentioned issues. Thus, we hope that our unique approach will provide a basis to gather the indispensable information of such flow which in turn helps various technological issues.

Mathematical formulation

Governing equations

A viscous, incompressible, steady hybrid nanofluid flow over a curved texture is assumed. The surface is presumed to be curved within the coiled configuration having radius R and curvilinear composition r and s. The stretching speed of the bended texture has been assumed to be in the form $U_w = as$ along s-direction; consequently, the stream constructs boundary layer regime through r-direction. Here, R defines the requisite distance from origin to the stretched surface, and most significantly, it describes the shape of the texture; that is, for elevated inputs of R the surface is shifted to flat from curved one. The geometrical schematic of our current investigation is revealed in Fig. 1. Here, hybrid nanofluid is the tiny composition of two different mixtures, namely ferrous $\left(Fe_3O_4\right)$ and graphene nanoparticles, along with host medium water. A uniform magnetic strength B_0 is employed normal to the surface. Throughout the investigation, we relied on some assumption like the absence of joule heating and viscous dissipation. Also, the presence of thermal slip and chemically reactive nanoparticles has been ignored. Nanofluids are in thermal equilibrium. Based on the above hypothesis, the indispensable leading equations of the desired system are arranged as follows [43, 44, 46, 47]:

$$\frac{\partial}{\partial r}\{(r+R)v\} + R\frac{\partial u}{\partial s} = 0, \tag{1}$$

$$\frac{u^2}{r+R} = \frac{1}{\rho_{\mathrm{hnf}}}\frac{\partial p}{\partial r}, \tag{2}$$

$$v\frac{\partial u}{\partial r} + \frac{R}{r+R}\left(u\frac{\partial u}{\partial s}\right) + \frac{1}{r+R}(uv) = -\frac{1}{\rho_{\mathrm{hnf}}}\frac{R}{r+R}\frac{\partial p}{\partial s} + \frac{\mu_{\mathrm{hnf}}}{\rho_{\mathrm{hnf}}}\left(\frac{\partial^2 u}{\partial r^2} + \frac{1}{r+R}\frac{\partial u}{\partial r} - \frac{u}{(r+R)^2}\right) - \frac{\sigma_{\mathrm{hnf}}B_0^2}{\rho_{\mathrm{hnf}}}u, \tag{3}$$

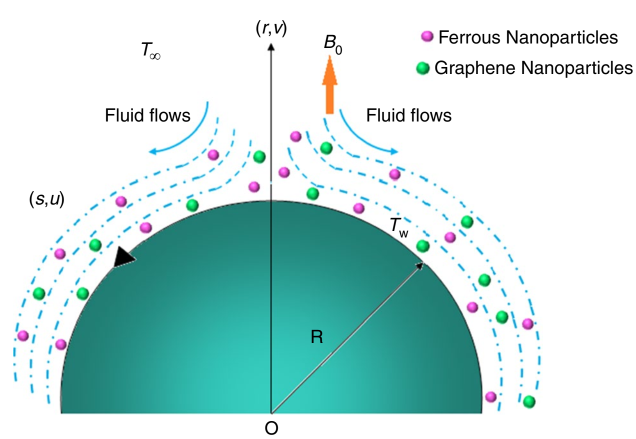

Fig. 1 Schematic of the flow

$$v\frac{\partial T}{\partial r}+\frac{R}{r+R}\left(u\frac{\partial T}{\partial s}\right)=\frac{\kappa_{\mathrm{hnf}}}{\left(\rho C_{\mathrm{p}}\right)_{\mathrm{hnf}}}\left(\frac{\partial^2 T}{\partial r^2}+\frac{1}{r+R}\frac{\partial T}{\partial r}\right)-\frac{1}{\left(\rho C_{\mathrm{p}}\right)_{\mathrm{hnf}}(r+R)}\frac{\partial}{\partial r}(r+R)q_{\mathrm{r}}+\frac{Q}{\left(\rho C_{\mathrm{p}}\right)_{\mathrm{hnf}}}\left(T-T_\infty\right). \tag{4}$$

Relevant boundary conditions are:

$$u=as+L\left(\frac{\partial u}{\partial r}-\frac{u}{r+R}\right), v=v_{\mathrm{w}}, -\kappa_{\mathrm{hnf}}\frac{\partial T}{\partial r}=h_{\mathrm{f}}\left(T_{\mathrm{w}}-T\right) \text{ at } r=0,$$
$$u\to 0, \frac{\partial u}{\partial r}\to 0, T\to T_\infty \text{ as } r\to\infty. \tag{5}$$

where p designates the nanofluid pressure. Here, it is also important to say that at the vicinity of the surface nanofluid acquires velocity such that $u=as+L\left(\frac{\partial u}{\partial r}-\frac{u}{r+R}\right)$ and $v=v_{\mathrm{w}}$ represents the suction/injection velocity for $v_{\mathrm{w}}<0$ and $v_{\mathrm{w}}>0$, respectively. Also, Q ensures the attendance of heat source/sink according as $Q>0$ and $Q<0$. If we presuppose optically thick boundary regime where Rosseland estimation can be incorporated, the radiative heat flux q_{r} becomes [51, 55, 56],

$$q_{\mathrm{r}}=-\frac{4\sigma^*}{3\kappa^*}\frac{\partial T^4}{\partial r}=-\frac{16\sigma^*}{3\kappa^*}T^3\frac{\partial T}{\partial r} \tag{6}$$

where σ^* is the Stephan–Boltzmann constant, κ^* is mean absorption coefficient. Now if we apply the non-dimensional expression of T as $\theta(\eta)=\frac{T-T_\infty}{T_{\mathrm{w}}-T_\infty}$ as in Eq. (6), we will have $T=T_\infty\left\{1+\left(\theta_{\mathrm{w}}-1\right)\theta\right\}$ where $\theta_{\mathrm{w}}=\frac{T_{\mathrm{w}}}{T_\infty}$.

Similarity conversion

To formulate the system dimensionless, we need to utilize the [43, 44, 46, 47]:

$$\eta=\sqrt{\frac{a}{v_{\mathrm{f}}}}r,\ u=asf'(\eta),\ v=-\frac{R}{r+R}\sqrt{av_{\mathrm{f}}}f(\eta),$$
$$\theta(\eta)=\frac{T-T_\infty}{T_{\mathrm{w}}-T_\infty},\ p=\rho_{\mathrm{f}}(as)^2P(\eta) \tag{7}$$

where η indicates as similarity variable.

Thermophysical features

Here, we maintain our investigation jointly for hybrid nanoliquid and ordinary unitary nanofluid. We have selected two tiny particles, namely Fe_3O_4 and Graphene, for hybrid nanoliquid and Fe_3O_4 stands for usual nanosolution (Table 1). To frame the hydrothermal interactions flawlessly, we have accumulated the leading equations using the thermophysical model for hybrid nanoliquid as explored by Takabi et al. [59] and Chamkha et al. [51]. It is crucial to address that introducing $\phi_2=0.0$ leads to unitary nanofluid model reported by Oztop and Abu-Nada [60] and Maxwell [61]. Those mathematical formulations are given in Table 2.

Table 1 Thermophysical properties of base fluid and nanoparticles [16, 17]

Physical properties	Water	Graphene	Fe_3O_4
C_{p} /J $\mathrm{Kg^{-1}\,K^{-1}}$	4180	2100	670
ρ/Kg $\mathrm{m^{-3}}$	997	2250	5180
κ/W $\mathrm{m^{-1}\,K^{-1}}$	0.6071	2500	9.7
$\sigma/\Omega^{-1}\mathrm{m^{-1}}$	0.005	10^7	25,000

Dimensionless appearance

Employing the conversion as in (7), governing Eqs. (1)–(4) together with boundary conditions in (5) are renewed into dimensionless form as follows:

$$P'=\frac{f'^2}{(\eta+K)}L_1 \tag{8}$$

$$\frac{2K}{\eta+K}\frac{1}{L_1}P-\frac{K}{(\eta+K)}ff''+\frac{K}{(\eta+K)}f'^2-\frac{K}{(\eta+K)^2}ff'-\frac{L_4}{L_1}\left(f'''+\frac{1}{(\eta+K)}f''-\frac{1}{(\eta+K)^2}f'\right)+\frac{L_5}{L_1}Mf'=0 \tag{9}$$

$$\theta''+\frac{\theta'}{(\eta+K)}+\frac{1}{(\eta+K)}\frac{4N}{3L_3}\frac{d}{\mathrm{d}\eta}\left\{(\eta+K)\left(1+\theta(\eta)\left(\theta_{\mathrm{w}}-1\right)\right)^3\frac{\mathrm{d}\theta(\eta)}{\mathrm{d}\eta}\right\}+\Pr\frac{L_2}{L_3}\left\{\frac{K}{(\eta+K)}f\theta'+\frac{\lambda\theta}{L_2}\right\}=0 \tag{10}$$

The prime reflects the differentiation w.r.t. η and

$$L_1=\frac{\rho_{\mathrm{hnf}}}{\rho_{\mathrm{f}}}, L_2=\frac{(\rho C_{\mathrm{p}})_{\mathrm{hnf}}}{(\rho C_{\mathrm{p}})_{\mathrm{f}}}, L_3=\frac{k_{\mathrm{hnf}}}{k_{\mathrm{f}}}, L_4=\frac{\mu_{\mathrm{hnf}}}{\mu_{\mathrm{f}}}, L_5=\frac{\sigma_{\mathrm{hnf}}}{\sigma_{\mathrm{f}}}.$$

Corresponding boundary conditions are transformed as,

$$f'(0)=1+L_{\mathrm{slip}}\left[f''(0)-\frac{f'(0)}{K}\right],$$
$$f(0)=S,\ \theta'(0)+\frac{\mathrm{Bi}}{L_3}(1-\theta(0))=0 \text{ at } \eta=0$$
$$f'\to 0, f''\to 0, \theta\to 0 \text{ as } \eta\to\infty. \tag{11}$$

where $S>0$ indicates suction and $S<0$ injection and $\lambda=\frac{Q}{a(\rho c_{\mathrm{p}})_{\mathrm{f}}}$ is the heat source/sink parameter according as $\lambda>0$ or $\lambda<0$.

Table 2 Thermophysical models of nanofluid and hybrid nanofluid [51, 59, 60]

Properties	Nanofluid (Fe_3O_4/water)
Density	$\rho_{nf} = (1-\phi)\rho_f + \phi\rho_s$
Heat capacity	$(\rho C_p)_{nf} = (1-\phi)(\rho C_p)_f + \phi(\rho C_p)_s$
Viscosity	$\mu_{nf} = \dfrac{\mu_f}{(1-\phi)^{2.5}}$
Thermal conductivity	$\dfrac{k_{nf}}{k_f} = \dfrac{k_s + (n-1)k_f - (n-1)\phi(k_f - k_s)}{k_s + (n-1)k_f + \phi(k_f - k_s)}$
Properties	Hybrid nanofluid (Fe_3O_4 *and* Graphene/water)
Density	$\rho_{hnf} = (1-\phi_1-\phi_2)\rho_f + \phi_1\rho_1 + \phi_2\rho_2$
Heat capacity	$(\rho C_p)_{hnf} = (1-\phi_1-\phi_2)(\rho C_p)_f + \phi_1(\rho C_p)_1 + \phi_2(\rho C_p)_2$
Viscosity	$\mu_{hnf} = \frac{\mu_f}{(1-\phi_1-\phi_2)^{2.5}}$
Thermal conductivity	$\dfrac{\kappa_{hnf}}{\kappa_f} = \left\{\dfrac{\kappa_1\phi_1+\kappa_2\phi_2}{\phi_1+\phi_2} + 2\kappa_f + 2(\kappa_1\phi_1+\kappa_2\phi_2) - 2(\phi_1+\phi_2)\kappa_f\right\} \times \left\{\dfrac{\kappa_1\phi_1+\kappa_2\phi_2}{\phi_1+\phi_2} + 2\kappa_f - 2(\kappa_1\phi_1+\kappa_2\phi_2) + (\phi_1+\phi_2)\kappa_f\right\}^{-1}$
Electrical conductivity	$\frac{\sigma_{hnf}}{\sigma_f} = 1 + \dfrac{3\left(\frac{\phi_1\sigma_1+\phi_2\sigma_2}{\sigma_f}\right) - 3(\phi_1+\phi_2)}{2 + \left\{\dfrac{\phi_1\sigma_1+\phi_2\sigma_2}{(\phi_1+\phi_2)\sigma_f}\right\} - \left\{\dfrac{\phi_1\sigma_1+\phi_2\sigma_2}{\sigma_f} - (\phi_1+\phi_2)\right\}}$

Here, 1 and 2 designate Fe_3O_4 and graphene nanoparticles, respectively

Eliminating the pressure term from (8) and (9), we have

$$f^{iv} + \frac{2}{(\eta+K)}f''' - \frac{1}{(\eta+K)^2}f'' + \frac{1}{(\eta+K)^3}f' + \frac{L_1}{L_4}\left(\begin{array}{c}\dfrac{K}{(\eta+K)}(ff''' - f'f'') + \dfrac{K}{(\eta+K)^2}(ff'' - f'^2) \\ -\dfrac{K}{(\eta+K)^3}ff' - \dfrac{L_5}{L_1}Mf'' - \dfrac{L_5}{L_1}\dfrac{M}{(\eta+K)}f'\end{array}\right) = 0. \tag{12}$$

Physical quantities

Frictional coefficient and Nusselt number are defined as:

$$C_f = \frac{\tau_w}{\rho_{hnf}(as)^2},\ \mathrm{Nu} = \frac{sq_w}{\kappa_f(T_w - T_\infty)}$$
$$\text{where } \tau_w = \mu_{hnf}\left(\frac{\partial u}{\partial r} - \frac{u}{r+R}\right)_{r=0} \text{ and } q_w = -\kappa_{nf}\left(\frac{\partial T}{\partial r}\right)_{r=0} + q_r|_{r=0} \tag{13}$$

Introducing the dimensionless variables as in (7), we acquire the reduced frictional coefficient and Nusselt number as follows:

$$C_{fr} = \sqrt{\mathrm{Re}_s}C_f = \left(\frac{(1-\phi_1-\phi_2)^{-2.5}}{(1-\phi_1-\phi_2) + \phi_1\left(\frac{\rho_1}{\rho_f}\right) + \phi_2\left(\frac{\rho_2}{\rho_f}\right)}\right)\left(f''(0) - \frac{1}{K}f'(0)\right) \tag{14}$$

$$\mathrm{Nu}_r = \frac{\mathrm{Nu}}{\sqrt{\mathrm{Re}_s}} = -\frac{\kappa_{hnf}}{\kappa_f}\left[1 + \frac{4N}{3L_3}\left\{1 + (\theta_w - 1)\theta(0)\right\}^3\right]\theta'(0) \tag{15}$$

Numerical procedure

Numerical method

The reduced Eqs. (8)–(12) are highly nonlinear and coupled in nature, and thus, their closed form solutions are not possible. They can be solved numerically using Runge–Kutta-4 (RK-4) with shooting method for different values of parameters. The proposed RK-4 method with shooting technique is not new method, but it has been used extensively by several researchers in dealing with the problems of boundary layer flows. Moreover, the shooting technique adopted is effective and results in high accuracy when compared to other methods. That is why, we used this method. In this work, we have used MAPLE-17 software to simulate the flow. The effects of the emerging parameters on the dimensionless velocity, temperature, skin friction and Nusselt number are studied. The step size is taken $\Delta\eta = 0.01$, and accuracy is up to the fifth decimal place as the criterion of convergence. We assumed a suitable finite value for the far-field boundary condition in (11), i.e. $\eta \to \infty$, say η_∞. The inner iteration is done with the convergence criterion of 10^{-6} in all cases.

Code of verification

Mehmood et al. [52] investigate the nanofluid flow over a convectively heated impermeable curved surface. They used Buongiorno model to simulate the flow, and viscous dissipation was considered by them. But, our model depicts the water-based Fe_3O_4–graphene nanofluid flow over a permeable slippery curved surface. Impacts of magnetic field, convective heat transfer, presence of heat source/sink and nonlinear thermal radiation have been included. Thus, we have extended the work of Mehmood et al. [52]. To verify the model's validity, we have extracted the reduced skin frictional values for various values of curvature parameter and the same is executed only for viscous fluid flow over curved surface. Mathematically, we have assembled our parametric values as $M = L_{\mathrm{slip}} = S = 0.0$. The numeric outcomes are listed in Table 3 and compared against Mehmood et al. [52] and Abbas et al. [53]. It shows excellent accord with previous investigation.

Table 3 Numerical values of the skin friction coefficient at $M=0$

K	Mehmood et al. [52]	Abbas et al. [53]	Present
5	– 1.15763	– 1.15763	– 1.15763121
10	– 1.07349	– 1.07349	– 1.07348861
20	– 1.03561	– 1.03561	– 1.03560983
30	– 1.02353	– 1.02353	– 1.02353108
40	– 1.01759	– 1.01759	– 1.01758661
50	– 1.01405	– 1.01405	– 1.01404923
100	– 1.00704	– 1.00704	– 1.00703844
200	– 1.00356	– 1.00356	– 1.00356418
1000	– 1.00079	– 1.00079	– 1.00079932
Infinity	– 1.00000	– 1.00000	– 1.00001049

Result and discussion

This section addresses the effect of the dynamic parameters on both hybrid nanofluid and usual nanofluid hydrothermal behaviour. Requisite graphs and tables have been shown to reveal the same. Numeric outputs of frictional factor and heat transport are calculated and reviewed. A detailed comparative discussion between usual and hybrid nanofluid is also brought to light to explore the hydrothermal variations of both liquids. We considered the parametric values as $K = 5.0$, $M = S = N = L_{\mathrm{slip}} = 0.2$, $\mathrm{Bi} = 0.5$, $\theta_{\mathrm{w}} = 1.2$, $\phi_1 = \phi_2 = 0.1$ unless otherwise mentioned.

Effect of curvature parameter (*K*)

Figure 2 explores the effect of curvature factor on velocity profile. Figure 2a shows the variations for suction and Fig. 2b for injection. Velocity has been detected to amplify for both usual nanofluid and hybrid nanofluid. The effects are not so prominent, but close view of the current scenario addresses that hybrid nanofluid acquires higher-velocity profile as compared to the usual one. Physically, non-dimensional definition of $K = R\sqrt{\frac{a}{\nu_{\mathrm{f}}}}$ allows us to predict that less kinematic viscous hindrance will be experienced for enhanced curvature factor. Thus, the fluid moves effortlessly. Additionally, it is noteworthy to observe that deviation in each curves is little bit less for injection as compared to suction. Figure 3b assures that the skin friction is reduced for increasing inputs of K. For hybrid nanofluid, frictional effect is comparatively higher than usual nanosuspension as given in Table 4. Figure 4 depicts pressure variations for both liquids. The green surface confirms hybrid nanofluid and blue surface designates the usual nanofluid. Also, the pressure amplifies as K enlarges. Figure 5a shows the temperature variations in suction.

Fig. 2 Effect of K on velocity

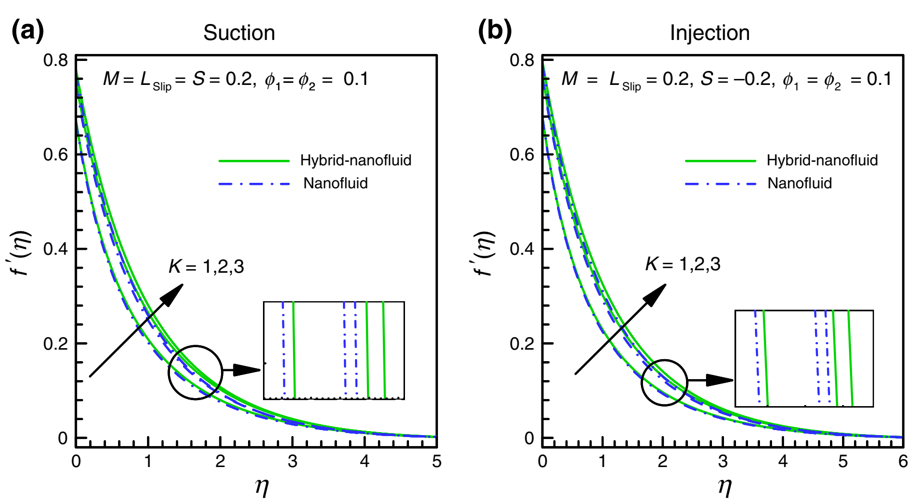

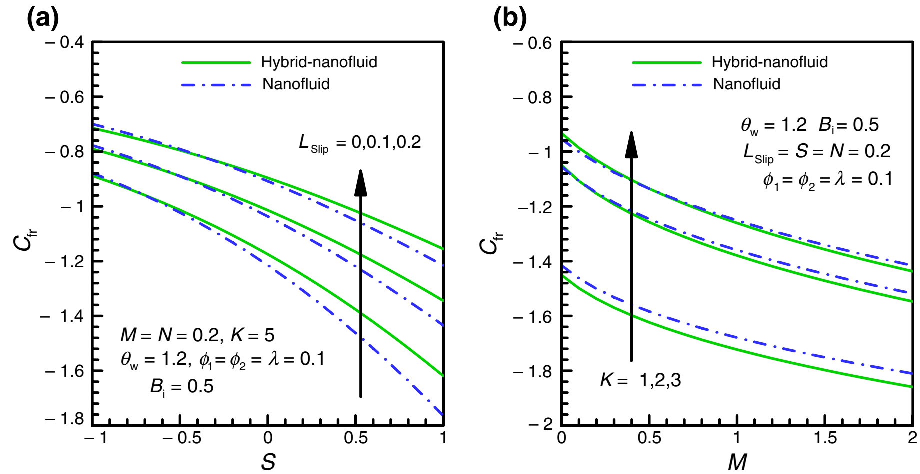

Fig. 3 Effect of S, L_{slip}, M, K on skin friction

Table 4 Variation of skin friction for different values of parameters at $\phi_2 = 0.1$

Parameters					C_{fr}	
ϕ_1	S	L_{slip}	M	K	Hybrid nanofluid	Nanofluid
0.0	0.2	0.2	0.2	5	−0.9057461	−0.8237879
0.1					−0.9420483	−0.9624192
0.2					−1.0403389	−0.9860888
0.1	−0.6				−0.7773916	−0.7706873
	−0.3				−0.8330200	−0.8346259
	0.0				−0.8959902	−0.9081264
	0.3				−0.9662683	−0.9910922
	0.6				−1.0434208	−1.0827231
	0.2	0.0			−1.2505216	−1.3073907
		1.0			−0.4964671	−0.4923507
		2.0			−0.3190479	−0.3129831
		0.2	0.0		−0.8839662	−0.8558153
			1.0		−1.1674311	−1.1662934
			2.0		−1.3481810	−1.3341938
			0.2	1.0	−1.5374468	−1.5007292
				2.0	−1.1536364	−1.1499423
				3.0	−1.0313759	−1.0311571

Temperature goes down for amplifying curvature factor. Effects are distinct. Initially, within $0.0 \le \eta \le 0.5$ usual nanofluid consumes higher temperature than hybrid nanoliquid. But, slightly away from the surface hybrid nanofluid exhibits the elevated thermal behaviour. It is expected because hybrid nanofluid succours double metallic nanoparticles within the host fluid. For injection in Fig. 5b, we perceive more distinct outlines of temperature as compared to suction because by injection more fluid enters inside the boundary region. Thus, the thermal performance becomes more pronounced. Heat transport in Fig. 6a and Table 5 ensures escalating behaviour for K. Comparatively, hybrid nanofluid exhibits higher heat transfer than conventional nanofluid.

Effect of magnetic parameter (M)

Figure 7a demonstrates the magnetic impact on hydrothermal variation of condensed nanofluid for suction, and Fig. 7b conveys the same for injection. In both cases, fluid velocity has been noted to decline owing to the presence of Lorentz force that transpires due to magnetic field. The consequences are well distinct for both fluids. Skin friction escalates for increasing M. Hybrid nanofluid illustrates higher drag affection. Thus, the surface will be less drag affected for hybrid nanofluid when magnetic strength varies rapidly. Table 4 expresses that the increasing rate is 32.03% for hybrid nanofluid, whereas for usual one it is 36.07%. Temperature in Fig. 8a, b shows linear relationship with M.

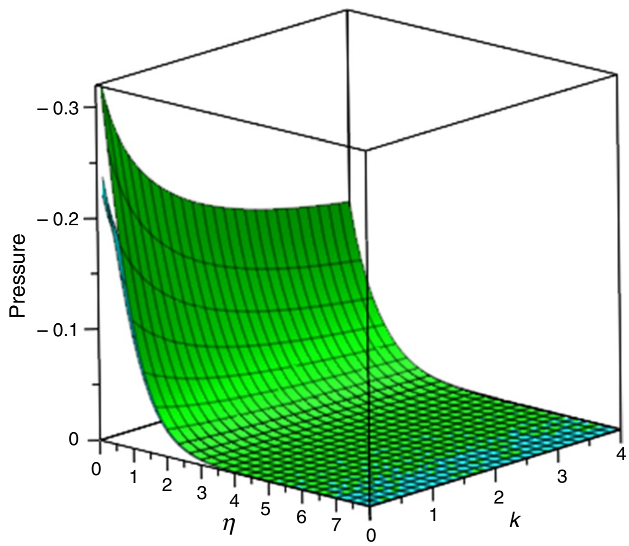

Fig. 4 Effect of K on pressure distribution for hybrid nanofluid versus usual nanofluid

The viscous hindrance generated due to M produces friction between fluid molecules and surface, which translates frictional energy into thermal energy. Hybrid nanofluid and injective nature of the sheet acquires high temperature as discussed in "Effect of curvature parameter (K)" section. Heat transfer drops off smoothly for magnetic effect in Fig. 6a. Table 5 authenticates that reduction rate is slower for hybrid nanosolution.

Effect of slip parameter (L_{slip})

The outcomes of velocity slip on the hydrothermal syndromes of both fluids are demonstrated in Figs. 9 and 10. Diminution in velocity is shown in Fig. 9a, b for both suction and injection, respectively. Prominent view is observed within $0.0 \le \eta \le 2.5$. In both situations, highest velocity is achieved for no-slip criteria. The reduced skin friction decreases for slip factor as depicted in Fig. 3a. Hybrid nanofluid provides highest frictional effect as compared to usual nanofluid, but initially slight reverse effect is noticed. The

Fig. 5 Effect of K on temperature

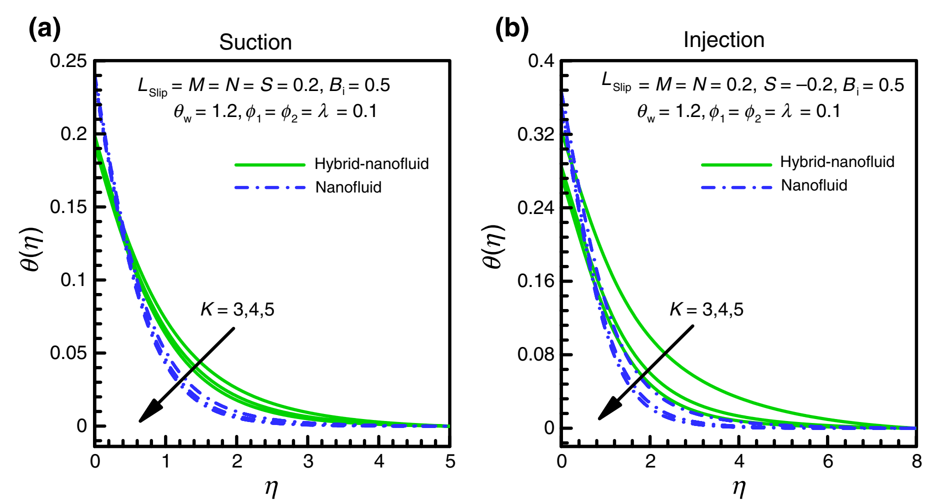

Fig. 6 Effect of $M, K, \mathrm{Bi}, N, \lambda, S$ on Nusselt number

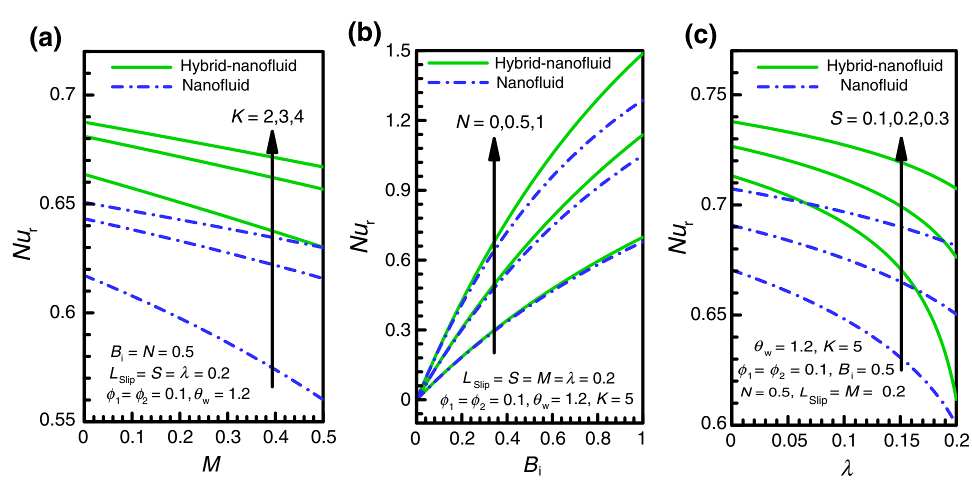

Table 5 Variation of Nusselt number for different values of parameters at $\phi_2 = 0.1$

Parameters									Nu_r	
ϕ_1	S	L_{slip}	M	N	B_i	λ	K	θ_w	Hybrid nanofluid	Nanofluid
0.0	0.2	0.2	0.2	0.2	0.2	0.1	5	1.2	0.235207	0.231975
0.1									0.237181	0.233302
0.2									0.238693	0.234518
0.1	−0.3								0.181150	0.172551
	−0.1								0.223855	0.214468
	0.0								0.230097	0.223275
	0.1								0.233226	0.225154
	0.3								0.239400	0.236352
	0.2	0.0							0.238813	0.235116
		1.0							0.230963	0.220168
		2.0							0.222574	0.217818
		0.2	0.0						0.237918	0.233852
			0.5						0.236115	0.232585
			1.0						0.233848	0.231493
			0.2	0.0					0.186704	0.184469
				0.3					0.262309	0.257528
				0.6					0.337223	0.329397
				0.2	0.5				0.540873	0.520582
					1.0				0.942588	0.880685
					2.0				1.496142	1.340164
					0.2	0.2			0.235694	0.230662
						0.3			0.222210	0.225758
						0.4			0.231410	0.216656
						0.3	2.0		0.222772	0.218786
							4.0		0.232397	0.222657
							6.0		0.236681	0.222830
							5.0	1.1	0.233305	0.225972
								1.4	0.237065	0.230753
								1.7	0.241056	0.236029

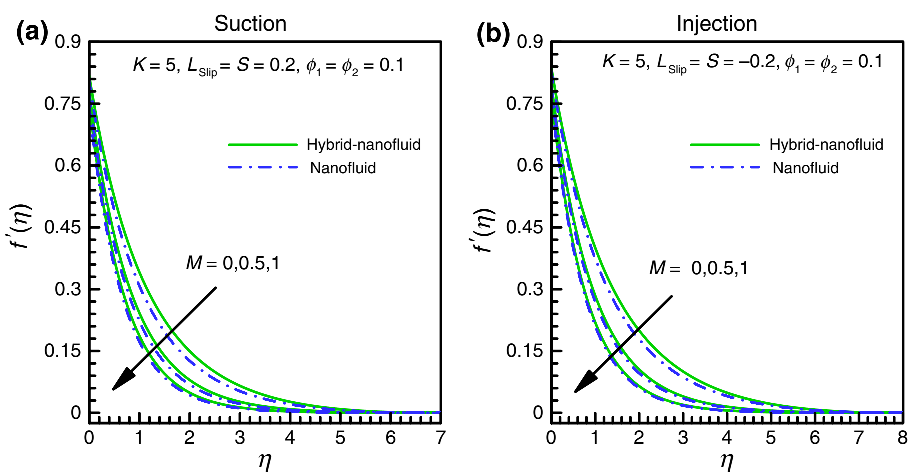

Fig. 7 Effect of M on temperature

reduction rate in Table 4 is 62.35% for hybrid nanofluid and 60.29% for ordinary nanoliquid. Temperature is increased due to the effect of L_{slip}. We observe distinct results in both suction and injection in Fig. 10a, b, respectively. Lower temperature is noted for no-slip criteria. For injection, near the surface effects are quite detectable. But, for suction, we note

Fig. 8 Effect of M on temperature

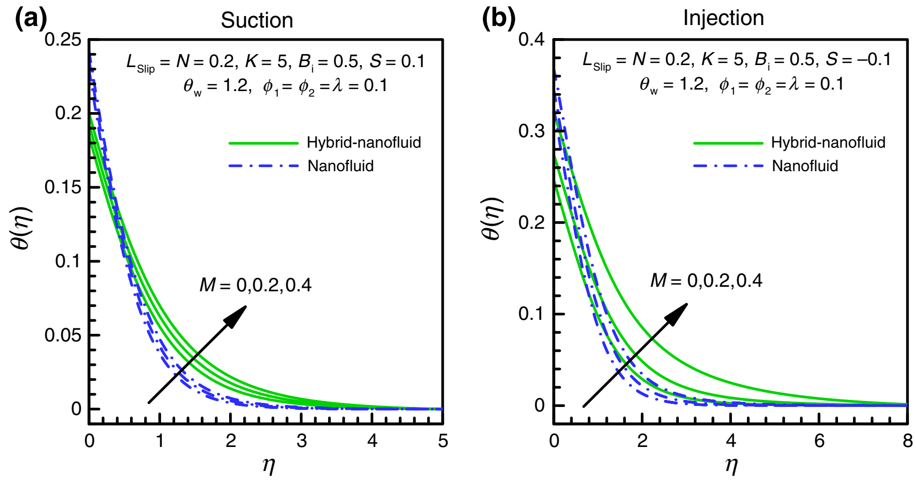

Fig. 9 Effect of L_{slip} on velocity

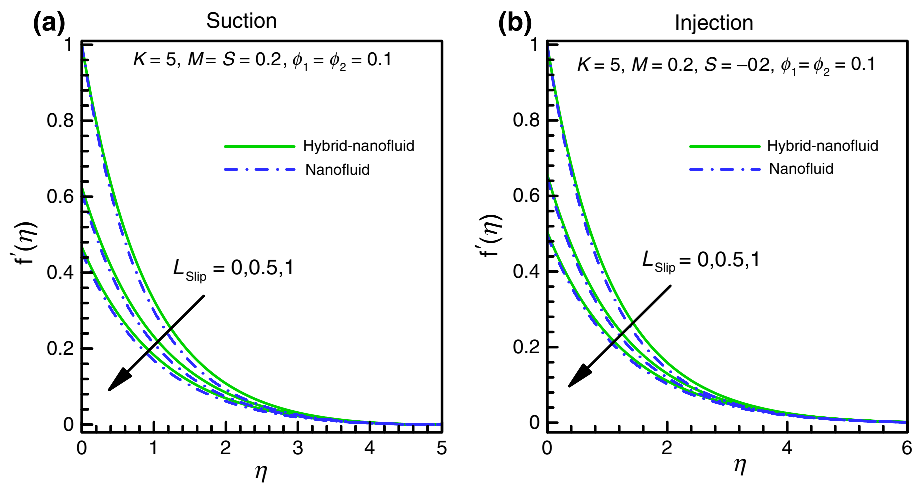

Fig. 10 Effect of L_{slip} on temperature

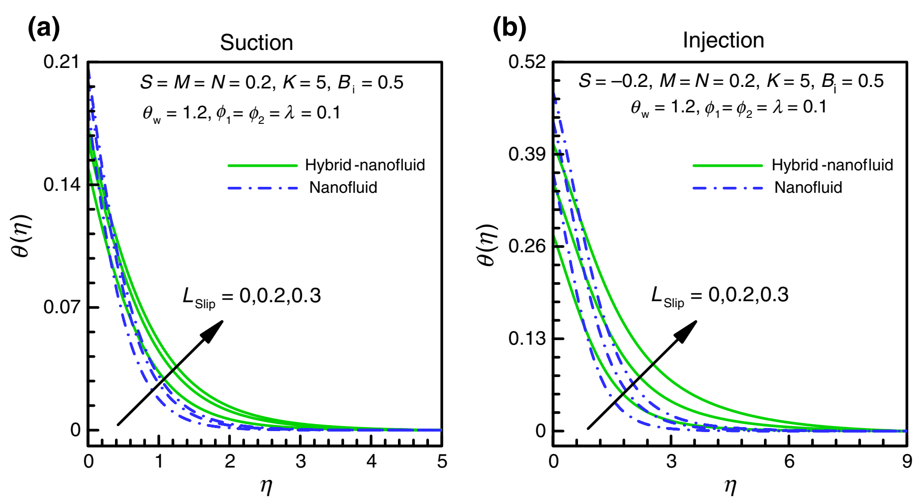

minor impact at the vicinity of the texture. Again, near the texture of the stretched sheet we mark that usual nanofluid depicts high thermal profile. Table 5 shows that Nusselt number drops off slightly. But, hybrid nanofluid explores less reduction profile as compared to usual one. Usual nanofluid exhibits 6.25% reduction in heat transport, whereas hybrid nanosolution confirms 3.28% reduction. Thus, cooling performance will be effective for hybrid nanofluid.

Effect of suction/injection parameter (S)

Effects of suction and injection on velocity profile are shown in Fig. 11a, b. Suction decreases the both fluids' velocities. Here, the impacts are well distinct. Clear outcome is detected within $0.0 \le \eta \le 3.0$. But, injection communicates totally reverse scenario. Most interestingly, the deviation between hybrid and usual nanofluid is not so effective under injection. Skin friction declines for suction and increase for injection. Figure 3a shows that skin friction declines for injection, but amplifies for suction. Initially injective texture confirms high drag affect for hybrid nanofluid, but when the texture started to alter from injection to suction, conventional nanofluid provides high friction. Such outcome or transition of result is noteworthy. Temperature increases for suction and injection.

Clear enhancement is shown in Fig. 12a, b. For injection, thermal enhancement is more pronounced than that of suction. Basically injection allows more nanofluid to enter inside the region, while for suction fluid leaves the region. Thus, the presence of more tiny metallic nanoparticles at the time of injection aids the system to consume more temperature. Near the texture usual nanoliquid shows high profile, but slightly away from it, such effects are reversed. Nusselt number amplifies in Fig. 6c for suction, and Table 5 exhibits reduction for injection. Table 5 ensures 19.54% increment in heat transfer for hybrid nanofluid in suction, whereas it is 19.07% for usual nanoliquid. Similarly, for injection the reduction in heat transfer is 2.68% and 4.98% for both hybrid and ordinary nanofluids, respectively. Thus, the cooling procedure is effective for hybrid nanofluid as compared to usual nanosuspension. Figure 13 displays the streamlines variations for both liquids under different modes of textures: injection, impermeable sheet and suction. Minor deviation in the trajectory is noted between the motions of the particles. Figure 14 addresses the comparative scenario of isotherms for both liquids. Here, the clear and distinct deviation is noted for both fluids.

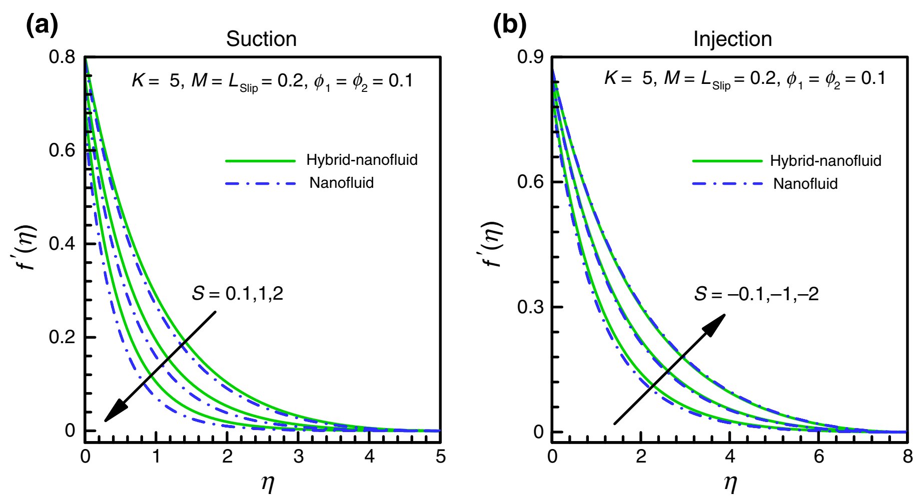

Fig. 11 Effect of S on velocity

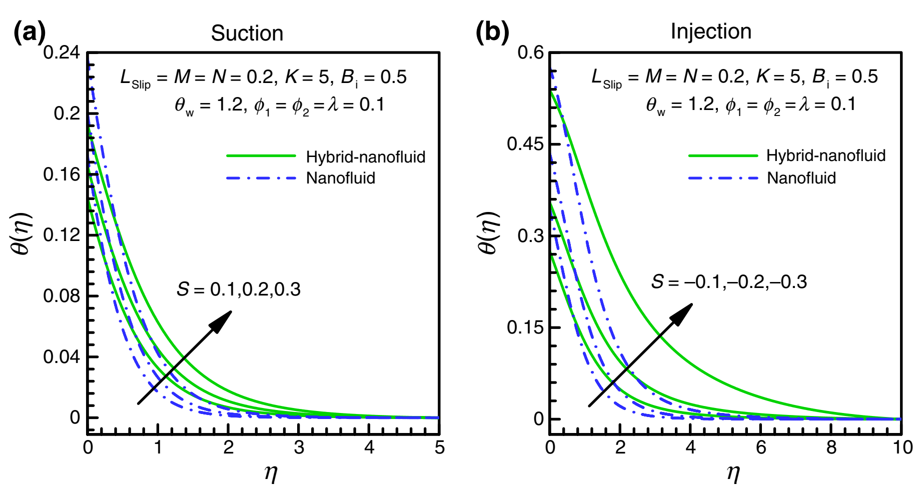

Fig. 12 Effect of S on temperature

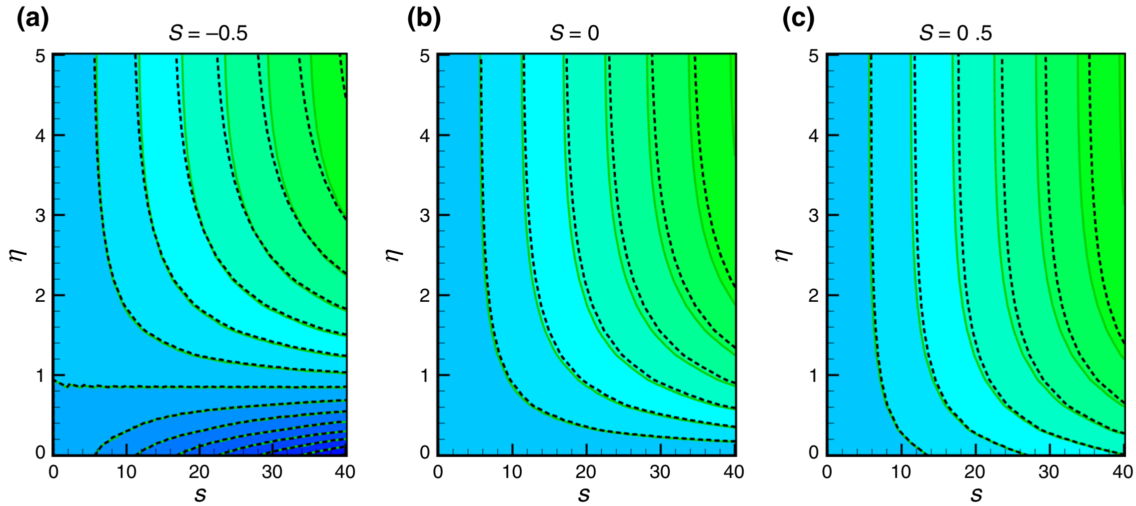

Fig. 13 Comparison of streamlines between hybrid nanofluid (solid line) and usual nanofluid (dashed line) for **a** injection, **b** impermeable sheet, **c** suction

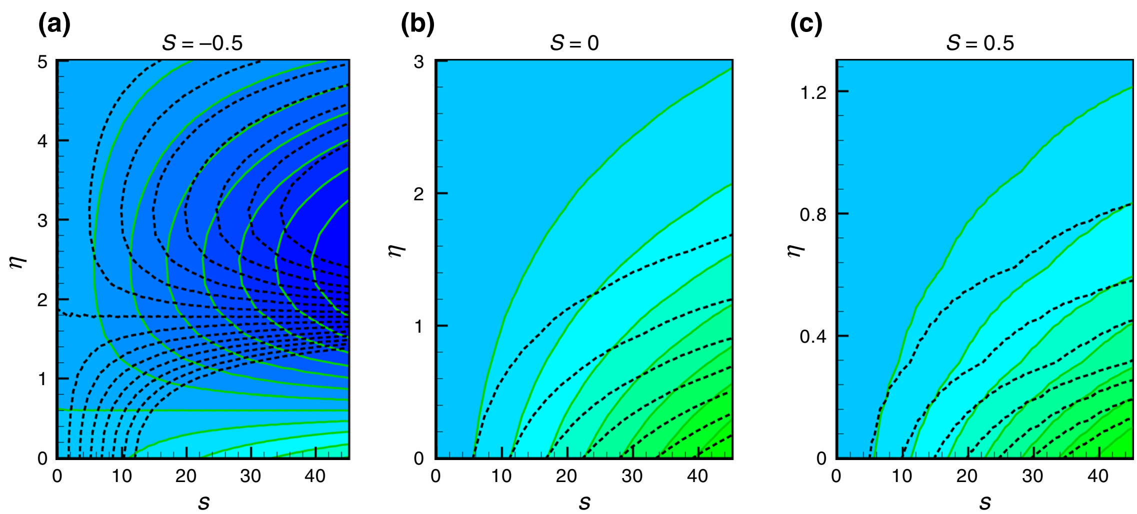

Fig. 14 Comparison of isotherms between hybrid nanofluid (solid line) and usual nanofluid (dashed line) for **a** injection, **b** impermeable sheet, **c** suction

Effect of radiation (N) and temperature ratio parameter $\left(\theta_w\right)$

The influence of radiation parameter (N) on the thermal profile is shown in Fig. 15. Figure 15a shows the thermal lines for suction and Fig. 15b for injection. Temperature is increased in both cases. Lowest output was ensured for the absence of radiation. Basically, increasing radiative aspects foster the molecular migration within the system, and thus, frequent collision between molecules translates into thermal energy. That is why temperature goes high. The presence of double tiny ingredients for hybrid solution makes such collision more random, and hence, the enhanced thermal profile is witnessed. Effects are distinct. Heat transfer is enhanced for radiation in Fig. 6b. Table 5 and Fig. 6b conclude that hybrid nanofluid becomes more efficient during this period. Same consequences are perceived for temperature ratio parameter $\left(\theta_w\right)$ via Fig. 16. Nusselt number in Fig. 17a, b due to θ_w illustrates escalating behaviour, but comparatively high impact in heat transfer is reported for injection.

Effect of thermal Biot number (Bi) and heat source/sink parameter (λ)

Temperature has been noticed to enlarge enormously in Fig. 18 for thermal Biot number. Same outcomes are

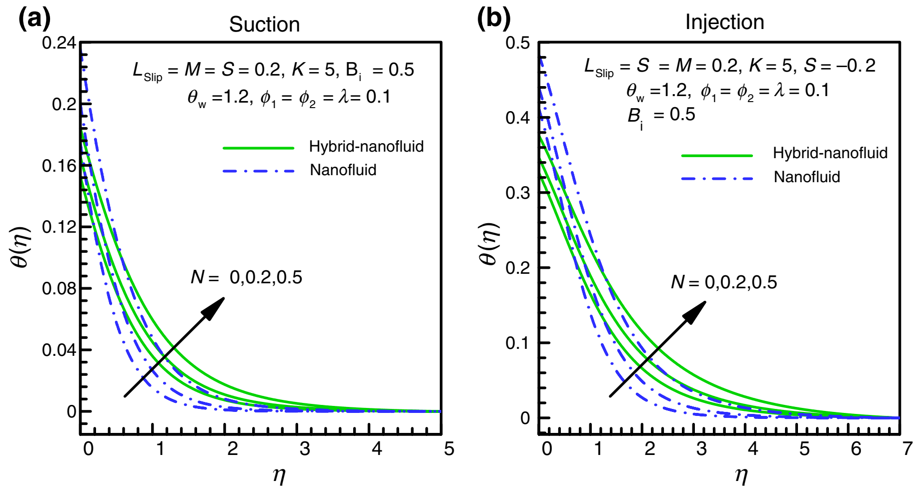

Fig. 15 Effect of N on temperature

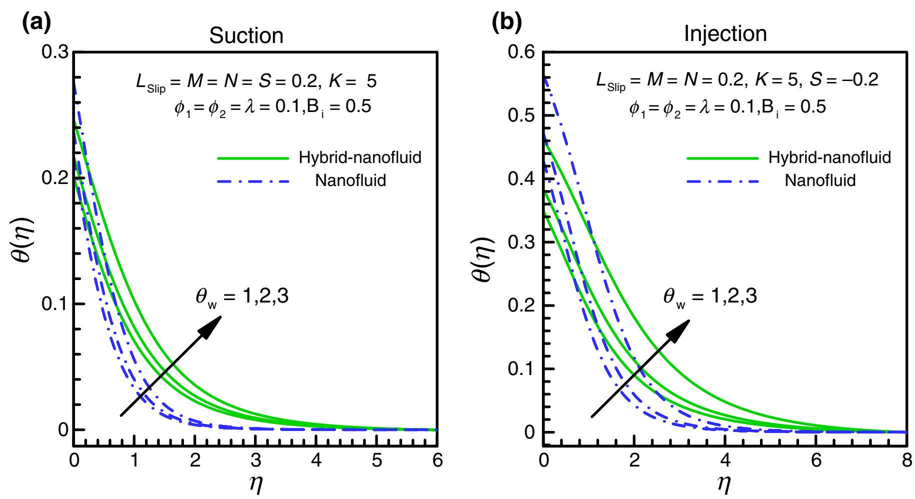

Fig. 16 Effect of θ_w on temperature

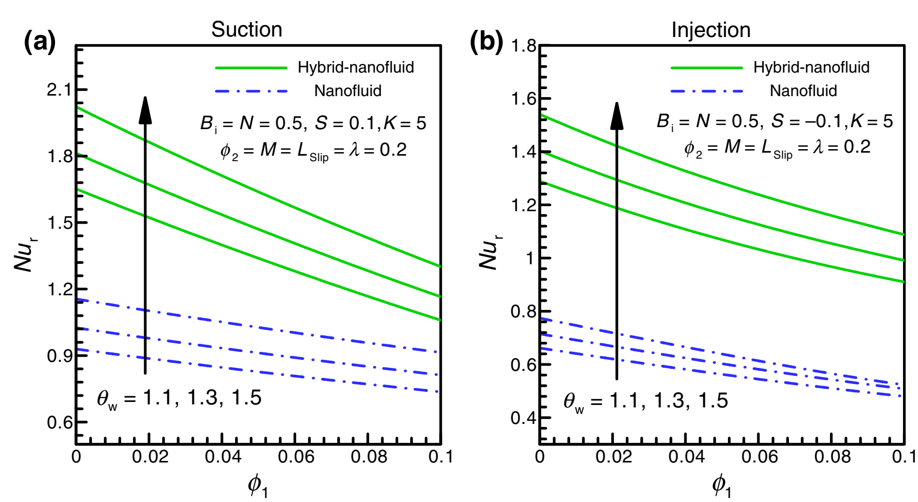

Fig. 17 Effect of θ_w, ϕ_1 on Nusselt number

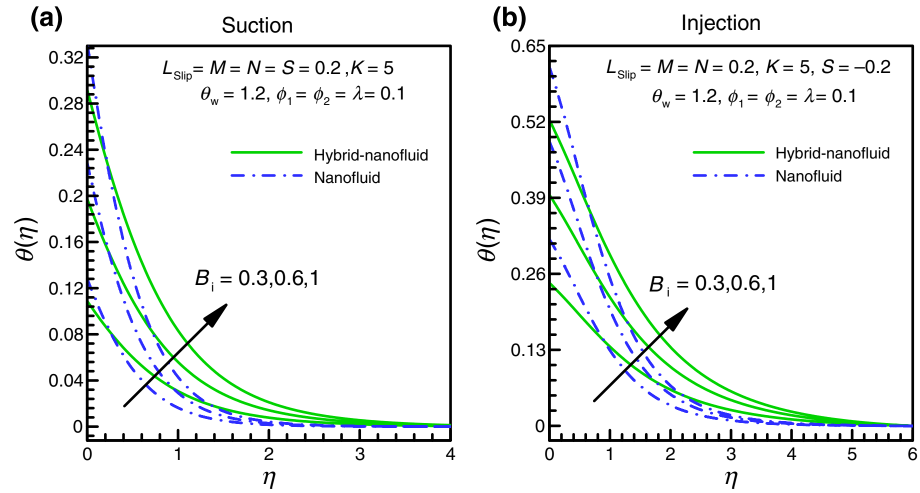

Fig. 18 Effect of Bi on temperature

acquired for suction and injection. As expected, near the surface ($0.0 \leq \eta \leq 0.5$) hybrid nanoliquid exhibits less thermal profile as compared to ordinary nanofluid. But, injective texture provides such effect slightly long. That means hybrid nanofluid continues to consume less temperature slightly away from the surface ($0.0 \leq \eta \leq 2.0$) during injection. After that, opposite situation comes into view. Nusselt number increases for Bi. Table 5 depicts 69.17% increment in heat transport for usual suspension, where it is 74.25% for hybrid nanofluid. The same is shown in Fig. 6b. The presence of heat source in Fig. 19a confirms thermal enhancement for both fluids. Near the surface, effects are striking. Also, here hybrid nanofluid explores impressive enhancement as compared to usual one. On the other side, heat sink in Fig. 19b demonstrated totally opposite outcomes. Reducing scenario is not so distinct inside the boundary region. Table 5 and Fig. 6c declare that heat transmission gets decreased for heat source. Figure 6c describes that at the beginning reduction rate was high for hybrid nanosolution, but at high intensity of heat source reverse consequences are perceived. Thus, for high magnitude of heat source hybrid nanofluid would be promising in cooling process.

Effect of nanoparticle concentration (ϕ_1)

Figure 20 explores the nanoparticle concentration effect on the velocity for suction and injection. In both cases, velocity gets flourished in response to the addition of tiny ingredients within the host fluid. Slightly away from the surface ($\eta > 1.5$), minor effects are detected. When concentration values are changed from $\phi_1 = 0.15 \rightarrow 0.25$, then slightly high fluctuation is achieved for hybrid nanofluid as compared to usual one. Skin friction is enhanced for such addition of tiny particles as given in Table 4. Temperature in Fig. 21 responds well for both suction and injection. Temperature increases for both forms of texture. As expected, hybrid nanofluid gets higher temperature because of double metallic ingredients inside the fluid. Near the vicinity, slight

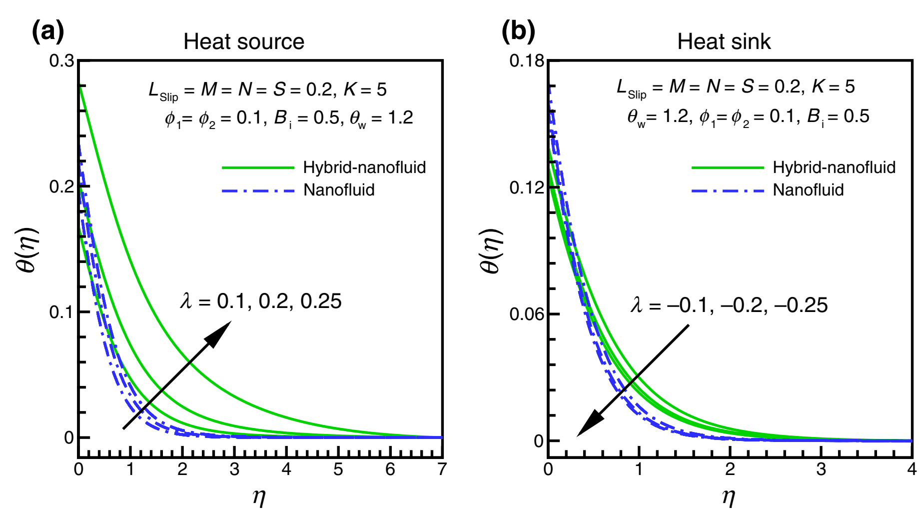

Fig. 19 Effect of λ on temperature

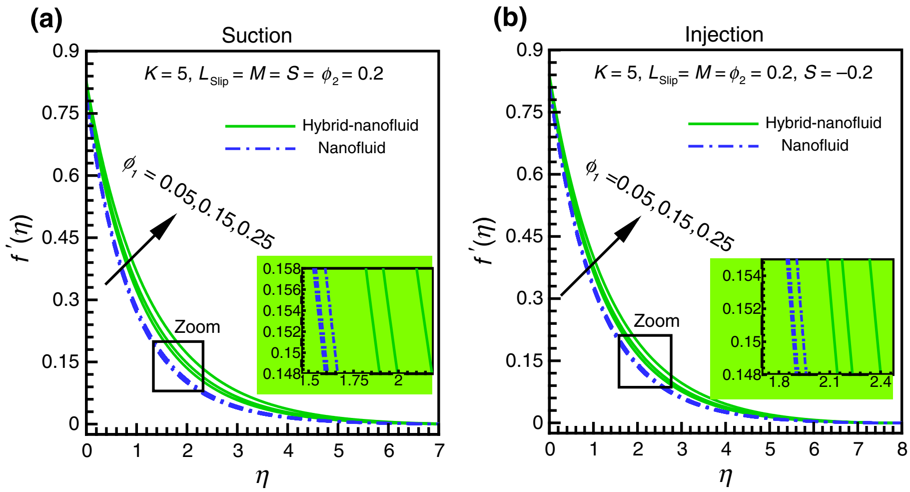

Fig. 20 Effect of ϕ_1 on velocity

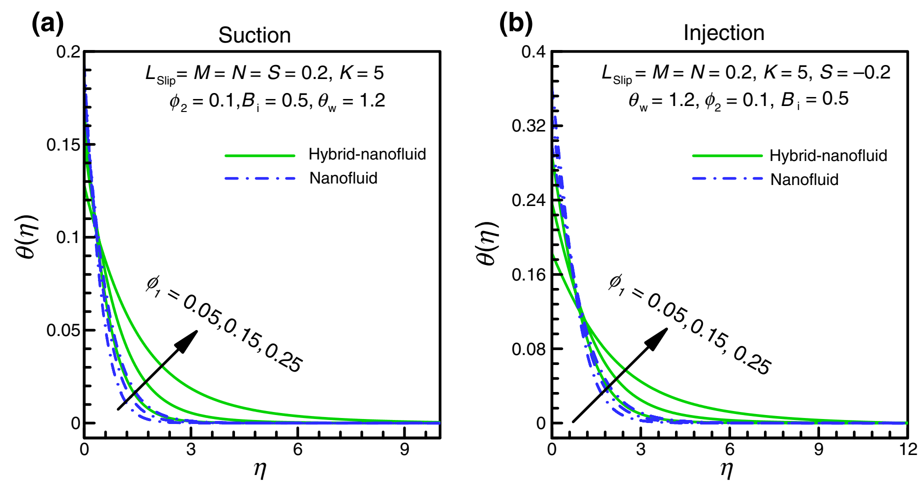

Fig. 21 Effect of ϕ_1 on temperature

reverse trend is marked for hybrid nanofluid during injection as shown in Fig. 21b. Heat transfer increases for both fluids, but faster enhancement given in Table 5 is for hybrid nanofluid as compared to the other. Hybrid nanofluid explores 0.83% increment, where conventional nanofluid declares 0.57% increment.

Conclusions

We investigated numerically a steady incompressible flow comprising hybrid nanofluid over a permeable bended structure of radius R. Ferrous and graphene nanoingredients along with water as base medium are considered as host fluid. Nonlinear thermal radiation and surface slip have been incorporated in this study. Additionally, the presence of heat sink/source is also guessed to be within the system. Shooting-based RK-4 scheme was employed to reveal the hydrothermal outcomes. Based on our study, the key points of the present analysis are highlighted as:

- The increment in magnetic parameter, suction and slip parameter leads to the diminution of flow velocity, while curvature factor, injection and nanoparticle concentration uplift it. Hybrid nanofluid exhibits comparatively higher-velocity profile than conventional nanofluid.
- Skin friction increases for magnetic parameter, suction and nanoparticle concentration, but reduces for curvature parameter, slip parameter and injection. Result depicts that highest increment in skin friction is produced by magnetic parameter and it is 32.03%. Also, usual nanofluid provides higher increment as compared to hybrid nanofluid. Thus, texture of the surface will be more drag affected for usual nanofluid. For magnetic field, it is almost 36.07%. Also, low reduction rate in skin friction is always produced by usual nanofluid. Highest reduction rate is marked for slip parameter where hybrid nanofluid conveys 62.35% reduction.
- Curvature parameter and heat sink decline the temperature, whereas others explore the opposite effect. The

presence of double additives increases temperature profile for hybrid nanofluid as compared to usual one.
- Magnetic parameter, velocity slip, injection and heat source reduce the heat transfer, while rest of the parameters fosters it. Our analysis portrays that hybrid nanofluid illustrates higher heat transport than conventional nanofluid. Cooling process becomes effective for hybrid nanofluid because of double tiny metallic nanoparticles. Impressive enhancement is assured for Biot number. For hybrid nanofluid, Biot number explores 74.25% increment and usual nanofluid conveys 69.17%. After that, radiation parameter and suction are the most influencing factor in heat transport. The result communicates that usual nanofluid fosters the reduction rate. Slip parameter assures highest reduction and it is almost 6.25%.

Acknowledgements The authors wish to express their cordial thanks to the respected Editor in chief and honourable reviewers for their valuable suggestions and comments to improve the presentation of this article.

References

1. Choi SUS. Enhancing thermal conductivity of fluids with nanoparticles. In: Siginer DA, Wang HP, editors. Developments and applications of non-Newtonian flows, vol. 66. New York: ASME; 1995.
2. Sajid MU, Ali HM. Recent advances in application of nanofluids in heat transfer devices: a critical review. Renew Sustain Energy Rev. 2019;103:556–92.
3. Khan MS, Abid M, Ali HM, Amber KP, Bashir MA, Javed S. Comparative performance assessment of solar dish assisted s-CO_2 Brayton cycle using nanofluids. Appl Therm Eng. 2019;148:295–306.
4. Esfe MH, Afrand M. A review on fuel cell types and the application of nanofluid in their cooling. J Therm Anal Calorim. 2020;140:1633–54.
5. Sheikholeslami M. New computational approach for exergy and entropy analysis of nanofluid under the impact of Lorentz force through a porous media. J Clean Prod. 2019;344:319–33.
6. Sheikholeslami M, Rezaeianjouybari B, Darzi M, Shafee A, Li Z, Nguyen TK. Application of nano-refrigerant for boiling heat transfer enhancement employing an experimental study. Int J Heat Mass Transf. 2019;141:974–80.
7. Sadeghi A, Amini Y, Saidi MH, Chakraborty S. Numerical modeling of surface reaction kinetics in electrokinetically actuated microfluidic devices. Anal Chim Acta. 2014;838:64–75.
8. Sadeghi A, Amini Y, Saidi MH, Yavari H. Shear-rate-dependent rheology effects on mass transport and surface reactions in biomicrofluidic devices. AIChE J. 2015;61:1912–24.
9. Abdollahi P, Sabet JK, Moosavian MA, Amini Y. Microfluidic solvent extraction of calcium: modeling and optimization of the process variables. Sep Purif Technol. 2020;231:115875.
10. Marsousi S, Sabet JK, Moosavian MA, Amini Y. Liquid–liquid extraction of calcium using ionic liquids in spiral microfluidics. Chem Eng J. 2019;356:492–505.
11. Sheikholeslami M, Jafaryar M, Shafee A, Babazadeh H. Acceleration of discharge process of clean energy storage unit with insertion of porous foam considering nanoparticle enhanced paraffin. J Clean Prod. 2020;261:121206.
12. Jahromi PF, Sabet JK, Amini Y. Ion-pair extraction-reaction of calcium using Y-shaped microfluidic junctions: an optimized separation approach. Chem Eng J. 2018;334:2603–15.
13. Sheikholeslami M, Haq R, Shafee A, Li Z. Heat transfer behavior of nanoparticle enhanced PCM solidification through an enclosure with V shaped fins. Int J Heat Mass Transf. 2019;130:1322–42.
14. Mabood F, Khan WA, Makinde OD. Hydromagnetic flow of a variable viscosity nanofluid in a rotating permeable channel with Hall effects. J Eng Thermophys. 2017;26:553–66.
15. Mabood F, Nayak MK, Chamkha AJ. Heat transfer on the cross flow of micropolar fluids over a thin needle moving in a parallel stream influenced by binary chemical reaction and Arrhenius activation energy. Eur Phys J. 2019;134(9):427.
16. Khan NS, Zuhra S, Shah Z, Bonyah E, Khan W, Islam S. Slip flow of Eyring–Powell nanoliquid film containing graphene nanoparticles. AIP Adv. 2018;8:115302.
17. Aly EH. Dual exact solutions of graphene–water nanofluid flow over stretching/shrinking sheet with suction/injection and heat source/sink: critical values and regions with stability. Powder Technol. 2019;342:528–44.
18. Ullah I, Waqas M, Hayat T, Alsaedi A, Khan MI. Thermally radiated squeezed flow of magneto-nanofluid between two parallel disks with chemical reaction. J Therm Anal Calorim. 2019;135:1021–30.
19. Acharya N, Das K, Kundu PK. Effects of aggregation kinetics on nanoscale colloidal solution inside a rotating channel: a thermal framework. J Therm Anal Calorim. 2019;138(1):461–77.
20. Animasaun IL, Koriko OK, Adegbie KS, Babatunde HA, Ibraheem RO, Sandeep N, Mahanthesh B. Comparative analysis between 36 nm and 47 nm alumina–water nanofluid flows in the presence of Hall effect. J Therm Anal Calorim. 2019;135(2):873–86.
21. Sajid MU, Ali HM. Thermal conductivity of hybrid nanofluids: a critical review. Int J Heat Mass Transf. 2018;126:211–34.
22. Kaska SA, Khalefa RA, Hussein AM. Hybrid nanofluid to enhance heat transfer under turbulent flow in a flat tube. Case Stud Therm Eng. 2019;13:100398.
23. Shah TR, Ali HM. Applications of hybrid nanofluids in solar energy, practical limitations and challenges: a critical review. Sol Energy. 2019;183:173–203.
24. Huminic G, Huminic A. Hybrid nanofluids for heat transfer applications—a state-of-the-art review. Int J Heat Mass Transf. 2018;125:82–103.
25. Esfe MH, Esfandeh S, Rejvani M. Modeling of thermal conductivity of MWCNT-SiO_2 (30:70%)/EG hybrid nanofluid, sensitivity analyzing and cost performance for industrial applications: an experimental based study. J Therm Anal Calorim. 2018;131:1437–47.
26. Derakhshan R, Shojaei A, Hosseinzadeh Kh, Nimafar M, Ganji DD. Hydrothermal analysis of magneto hydrodynamic nanofluid flow between two parallel by AGM. Case Stud Therm Eng. 2019;14:100439.
27. Pandey AK, Kumar MM. Effect of viscous dissipation and suction/injection on MHD nanofluid flow over a wedge with porous medium and slip. Alex Eng J. 2016;55:3115–23.
28. Zeeshan A, Ellahi R, Mabood F, Hussain F. Numerical study on bi-phase coupled stress fluid in the presence of Hafnium and metallic nanoparticles over an inclined plane. Int J Numer Methods Heat Fluid Flow. 2019;29:2854–69.
29. Acharya N, Das K, Kundu PK. Rotating flow of carbon nanotube over a stretching surface in the presence of magnetic field: a comparative study. Appl Nanosci. 2018;8(3):369–78.
30. Ahmad R, Mustafa M, Hayat T, Alsaedi A. A numerical study of MHD nanofluid flow and heat transfer past a bidirectional exponentially stretching sheet. J Magn Magn Mater. 2016;407:69–74.

31. Manjunatha S, Kuttan BA, Jayanthi S, Chamkha AJ, Gireesha BJ. Heat transfer enhancement in the boundary layer flow of hybrid nanofluids due to variable viscosity and natural convection. Heliyon. 2019;5(4):e01469.
32. Hayat T, Nadeem S. Heat transfer enhancement with Ag–CuO/water hybrid nanofluid. Results Phys. 2017;7:2317–24.
33. Yousefi M, Dinarvand S, Yazdi ME, Pop I. Stagnation-point flow of an aqueous titania-copper hybrid nanofluid toward a wavy cylinder. Int J Numer Methods Heat Fluid Flow. 2018;28(7):1716–35.
34. Afridi MI, Tlili I, Goodarzi M, Osman M, Khan NA. Irreversibility analysis of hybrid nanofluid flow over a thin needle with effects of energy dissipation. Symmetry. 2019;11(5):663.
35. Nadeem S, Hayat T, Khan AU. Numerical study on 3D rotating hybrid SWCNT/MWCNT flow over a convectively heated stretching surface with heat generation/absorption. Phys Scr. 2019;94:075202.
36. Dinarvand S, Rostami MN, Pop I. A novel hybridity model for TiO_2–CuO/water hybrid nanofluid flow over a static/moving wedge or corner. Sci Rep. 2019;9:16290.
37. Acharya N, Bag R, Kundu PK. Influence of Hall current on radiative nanofluid flow over a spinning disk: a hybrid approach. Phys E Low Dimens Syst Nanostruct. 2019;111:103–12.
38. Devi SSU, Devi SPA. Numerical investigation of three-dimensional hybrid Cu Al_2O_3/water nanofluid flow over a stretching sheet with effecting Lorentz force subject to Newtonian heating. Can J Phys. 2016;94(5):490–6.
39. Acharya N, Bag R, Kundu PK. On the impact of nonlinear thermal radiation on magnetized hybrid condensed nanofluid flow over a permeable texture. Appl Nanosci. 2019. https://doi.org/10.1007/s13204-019-01224-w.
40. Acharya N, Maity S, Kundu PK. Influence of inclined magnetic field on the flow of condensed nanomaterial over a slippery surface: the hybrid visualization. Appl Nanosci. 2020;10:633–47.
41. Ali A, Saleem S, Mumraiz S, Saleem A, Awais M, Marwat DNK. Investigation on TiO_2–Cu/H_2O hybrid nanofluid with slip conditions in MHD peristaltic flow of Jeffrey material. J Therm Anal Calorim. 2020. https://doi.org/10.1007/s10973-020-09648-1.
42. Hassan M, Marin M, Ellahi R, Alamri SZ. Exploration of convective heat transfer and flow characteristics synthesis by Cu–Ag/water hybrid nanofluids. Heat Transf Res. 2018;49(18):1837–48.
43. Sajid M, Ali N, Javed T, Abbas Z. Stretching a curved surface in a viscous fluid. Chin Phys Lett. 2010;27:024703.
44. Sanni KM, Asghar S, Jalil M, Okechi NF. Flow of viscous fluid along a nonlinearly stretching curved surface. Results Phys. 2017;7:1–4.
45. Shaiq S, Maraj EN. Role of the induced magnetic field on dispersed CNTs in propylene glycol transportation toward a curved surface. Arab J Sci Eng. 2019;44:7515–28.
46. Imtiaz M, Hayat T, Alsaedi A. Convective flow of ferrofluid due to a curved stretching surface with homogeneous heterogeneous reactions. Powder Technol. 2017;310:154–62.
47. Afridi MI, Alkanhal TA, Qasim M, Tlili I. Entropy generation in Cu–Al_2O_3–H_2O hybrid nanofluid flow over a curved surface with thermal dissipation. Entropy. 2019;21:941.
48. Saba F, Ahmed N, Hussain S, Khan U, Mohyud-Din ST, Darus M. Thermal analysis of nanofluid flow over a curved stretching surface suspended by carbon nanotubes with internal heat generation. Appl Sci. 2018;8:395.
49. Acharya N. Active–passive controls of liquid di-hydrogen monoxide based nanofluidic transport over a bended surface. Int J Hydrogen Energy. 2019;44(50):27600–14.
50. Acharya N, Bag R, Kundu PK. On the mixed convective carbon nanotube flow over a convectively heated curved surface. Heat Transf. 2020. https://doi.org/10.1002/htj.21687.
51. Chamkha AJ, Dogonchi AS, Ganji DD. Magneto-hydrodynamic flow and heat transfer of a hybrid nanofluid in a rotating system among two surfaces in the presence of thermal radiation and Joule heating. AIP Adv. 2019;9:025103.
52. Mehmood Z, Iqbal Z, Azhar E, Maraj EN. Nanofluidic transport over a curved surface with viscous dissipation and convective mass flux. Z Naturforsch. 2016;72(3):223–9.
53. Abbas Z, Naveed M, Sajid M. Heat transfer analysis for stretching flow over a curved surface with magnetic field. J Eng Thermophys. 2013;22(4):337–45.
54. Imtiaz M, Mabood F, Hayat T, Alsaedi A. Homogeneous–heterogeneous reactions in MHD radiative flow of second grade fluid due to a curved stretching surface. Int J Heat Mass Transf. 2019;145:118781.
55. Ullah I, Hayat T, Alsaedi A, Asghar S. Dissipative flow of hybrid nanoliquid (H_2O–aluminum alloy nanoparticles) with thermal radiation. Phys Scr. 2019;94(12):125708.
56. Makinde OD, Mabood F, Ibrahim SM. Chemically reacting on MHD boundary layer flow of nanofluids over a nonlinear stretching sheet with heat source/sink and thermal radiation. Therm Sci. 2018;22:495–506.
57. AnanthaKumar K, Sandeep N, Sugunamma V, et al. Effect of irregular heat source/sink on the radiative thin film flow of MHD hybrid ferrofluid. J Therm Anal Calorim. 2020;139:2145–53.
58. Acharya N. On the flow patterns and thermal behaviour of hybrid nanofluid flow inside a microchannel in presence of radiative solar energy. J Therm Anal Calorim. 2019. https://doi.org/10.1007/s10973-019-09111-w.
59. Takabi B, Gheitaghy AM, Tazraei P. Hybrid water-based suspension of Al2O3 and Cu nanoparticles on laminar convection effectiveness. J Thermophys Heat Transf. 2016;30(3):523–32.
60. Oztop HF, Abu-Nada E. Numerical study of natural convection in partially heated rectangular enclosures with nanofluids. Int J Heat Fluid Flow. 2008;29:1326–36.
61. Maxwell J. A treatise on electricity and magnetism. 2nd ed. Cambridge: Oxford University Press; 1904.